

Solvothermal Synthesis of Oxamate-Based Helicate: Temperature Dependence of the Hydrogen Bond Structuring in the Solid

Laurent Lisnard,^{§,†} Lise-Marie Chamoreau,^{§,‡} Yanling Li,^{§,†} and Yves Journaux^{*,§,†}

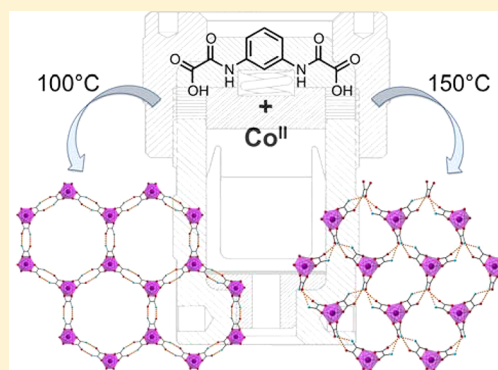
[§]Institut Parisien de Chimie Moléculaire, UPMC Univ Paris 06, Paris 75005, France

[†]CNRS, Institut Parisien de Chimie Moléculaire, UMR 7201, Paris 75005, France

[‡]Centre de résolution structurale, Institut Parisien de Chimie Moléculaire, Paris 75005, France

S Supporting Information

ABSTRACT: Solvothermal synthesis has been successfully tested as a new synthetic method toward the formation of oxamate-based coordination compounds. The reaction of 1,3-benzenedioxamic acid (H₄mpba) with divalent metal ions has afforded the dinuclear compounds TBA₂[Co₂(H₂mpba)₃·2DMF·5H₂O (1a), (HNEt₃)₂[Co₂(H₂mpba)₃·6DMF·5H₂O (1b), TBA₂[Ni₂(H₂mpba)₃·2DMF·2.5H₂O (2), and (HNEt₃)₂[Co₂(H₂mpba)₃] (3). Although the 3:2 ligand to metal ratio is known for the (mpba)⁴⁻ ligand under bench conditions, these complexes are the first examples of oxamate-based helicate. Furthermore, crystallographic studies show a temperature-dependent hydrogen bond structuring that leads to racemic or chiral hexagonal 3D networks.



INTRODUCTION

The synthesis of molecular building blocks that self-assemble or are capable of connexion with another component to form molecular objects or networks of defined topology or geometry is one of the major subjects in crystal engineering^{1,2} and in supramolecular chemistry.^{3–5} The assembly process relies on weak chemical interactions such as H-bonds, electrostatic interactions, or coordination bonding. However, due to subtle equilibria between these weak interactions, there are still many surprises in the outcome and the final product can be quite different from the expected one. These unexpected results often open up new opportunities and contribute greatly to the beauty of synthetic chemistry. Among all the research work on the crystal engineering of nets, the synthesis of metal–organic frameworks has increased exponentially.⁶ The reason for this success is related to the chemical flexibility of these materials owing to the presence of tunable organic and inorganic parts, which allows one to scale up the system or to introduce new properties. Moreover MOFs have many potential applications in catalysis but also in hydrogen⁷ and CO₂⁸ storage, which are two of the most pressing technological social needs. MOFs are also highly interesting for their physical properties such as luminescence^{9,10} or ferroelectricity¹¹ and magnetism.¹² Regarding magnetic MOFs, the goal is the obtainment of magnets and more precisely porous magnets, so in addition to the control over atom arrangement, the ability of organic ligands to propagate the electronic interaction between the magnetic ions is of paramount importance. At first sight, large porosity seems incompatible with magnetic ordering due to the exponential decrease of the interaction between the magnetic ions with

growing metal–metal distances^{13,14} inevitably leading to a dramatic drop in the ordering temperature value when the system is scaled up with longer organic linkers. To tackle this problem, we have designed over the past few years new polytopic oxamate-based ligands able to efficiently transmit electronic interaction across extended aromatic bridges via a spin polarization mechanism. Starting from these ligands, we were able to obtain homometallic polynuclear complexes that effectively exhibit relatively strong ferromagnetic interactions despite large metal–metal separation.^{15–18} When reacted with additional metal ions, some of these complexes give 2D or 3D magnetic MOFs^{19–21} with magnetic ordering in the 6.5 to 22.5 K temperature range. The metal–metal distance through the bridging oxamate ligand is not tunable but with the help of serendipity large octagonal pores have been obtained.²¹ Furthermore these networks are resizable by changing the aromatic parts while retaining a significant interaction. Nevertheless the final geometry of the nets depends on subtle chemical equilibria, and to fully exploit this family of ligands, we have decided to explore their reactivity in solvothermal conditions. This method imposes strong constraints both in pressure and in temperature to the reaction media and allows its user to work beyond the solvent's boiling point.²² Consequently the solubility and the mobility of the reactants are increased, and reactions that could not be accomplished or would not yield crystals under bench conditions become

Received: June 29, 2012

Revised: August 20, 2012

Published: September 4, 2012

feasible.²³ This method has convincingly proven its efficiency for the synthesis of multidimensional materials^{24,25} as well as the synthesis of coordination clusters²⁶ and represents therefore a convenient tool to investigate polyoxamate's reactivity.

To start our study, we have been focusing on the 1,3-benzenedioxamate ligand (Figure 1a) since it is known to

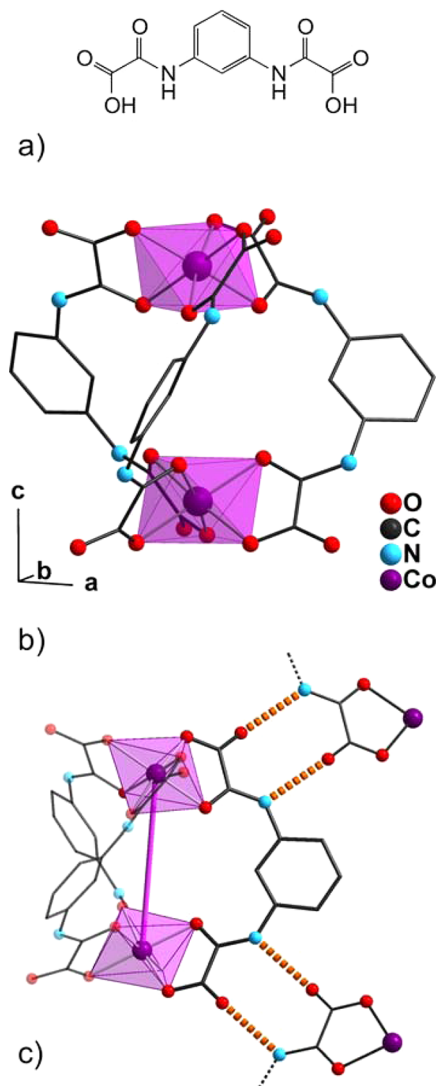


Figure 1. (a) Representation of the 1,3-benzenedioxamic acid; (b) structure of the anionic complex in **1b**, with legend as an inset, H atoms are omitted for clarity; (c) representation of the N(H)⋯O bond (orange dotted lines) between adjacent molecules in **1b**; H atoms are omitted for clarity; the dinuclear complex is schemed with an intramolecular Co–Co bound pictured in purple.

promote ferromagnetic exchange between paramagnetic ions through a spin polarization mechanism.¹⁵ We have thus reacted this ligand with cobalt(II) or nickel(II) salts in DMF varying the temperature of the solvothermal treatment. Reactions performed at 100 °C in the presence of TBAOH or NEt₃ have yielded the bimetallic compounds TBA₂[Co₂(H₂mpba)₃]-2DMF·5H₂O (**1a**), (HNEt₃)₂[Co₂(H₂mpba)₃]-6DMF·5H₂O (**1b**), and TBA₂[Ni₂(H₂mpba)₃]-2DMF·2.5H₂O (**2**), whereas the compound (HNEt₃)₂[Co₂(H₂mpba)₃] (**3**) has been obtained at 150 °C in the presence of triethylamine. Crystallographic studies reveal that all the complexes adopt a

helicate geometry, which has never been observed to date in oxamate-based complexes. X-ray diffraction studies also show that the supramolecular hydrogen-bond arrangement of the complexes in the solid is strongly dependent on the reaction temperature: reactions performed at 100 °C have afforded a racemic hexagonal 3D structure in contrast to a chiral phase that forms at 150 °C.

EXPERIMENTAL SECTION

Materials and Methods. All reagents were used as purchased with no further purification. Diethyl *N,N'*-1,3-benzenedioxamate (H₂Et₂mpba) was prepared according to the literature procedure.²⁷ ¹H and ¹³C NMR spectra were collected on a 400 MHz Bruker Avance spectrometer at 298 K. ATR/FT-IR spectra were collected on a Bruker TENSOR 27 equipped with a simple reflection ATR diamond plate of the Harrick MPV2 series. Magnetic measurements in dc mode were performed on a Quantum Design MPMS SQUID on polycrystalline samples restrained in a plastic film. Data were corrected for the diamagnetism contributions of the samples using Pascal constants. The sample holder diamagnetism was measured and subtracted from the raw data.

Synthesis. *Synthesis of H₄mpba·3H₂O.* Hydrate *N,N'*-1,3-benzenedioxamic acid was prepared as follows: aqueous NaOH (6.22 g, 1.55 mol, 100 mL) was added dropwise to a suspension of H₂Et₂mpba (12 g, 38.9 mmol) in water (800 mL). The solution was stirred for 30 min and filtered. Addition of 4 M HCl (38.9 mL, 1.55 mol) to the resulting solution leads to the formation of a white precipitate. After 15 min, the precipitate is collected on a sintered glass filter, washed with water and then with 50% v. EtOH, and dried for several hours in air and overnight at 45 °C in an oven. Yield: 10.9 g (91.5%). ¹H NMR (Bruker Avance 300 MHz, DMSO-*d*₆, 298 K) δ 10.74 (s, 2H, NH), 8.27 (s, 1H), 7.50 (d, 2H, *J* = 7.95 Hz), 7.34 (t, 1H, *J* = 8.1 Hz). ¹³C NMR (Bruker Avance 400 MHz, DMSO-*d*₆, 298K) δ 112.68, 116.83, 128.86, 137.83, 157.02, 162.11. IR (ATR, cm⁻¹): 3427 s; 3311 m; 3092 s; 2523 s; 1998 s; 1675 S; 1612 m; 1550 m; 1479 s; 1457 s; 1286 m; 1258 m; 1225 S; 1209 m; 1179 s; 1147 s; 1097 s; 993 s; 926 s; 875 s; 822 s; 787 m; 729 S; 678 s; 534 m; 500 m; 408 S; 262 S. Elemental analysis (%) calculated for C₁₀H₁₄N₂O₉ (*M*_r = 306.22 g mol⁻¹): C 39.22, H 4.60, N 9.14. Found: C 39.21, H 4.44, N 9.07.

*Synthesis of TBA₂[Co₂(H₂mpba)₃]-2DMF·5H₂O, **1a.*** CoCl₂·6H₂O (0.119 g, 0.5 mmol), H₂Et₂mpba (0.153 g, 0.5 mmol), and TBAOH (1 M in MeOH, 1 mL, 1 mmol) were placed in a 23 mL Teflon-lined autoclave filled with DMF (8 mL) and heated at 100 °C for 12 h. After slow cooling to room temperature, pink crystals of **1a** were collected, washed by sonication in DMF, and dried in air. Yield: 0.152 g (39%, based on Co). IR (ATR, cm⁻¹): 3470 s; 3197 s; 3197 s; 3083 s; 2963 s; 2875 s; 1661 S; 1624 S; 1595 S; 1543 S; 1474 S; 1456 m; 1409 s; 1364 S; 1294 m; 1255 s; 1228 s; 1171 s; 1093 s; 1062 s; 1031 s; 988 s; 934 s; 893 S; 837 s; 798 S; 760 s; 739 s; 690 s; 660 s; 598 s; 539 s; 515 s; 473 s; 445 m; 404 s; 357 s; 305 m; 254 S. Elemental analysis (%) calculated for C₆₈H₁₁₄Co₂N₁₀O₂₅ (*M*_r = 1589.55 g mol⁻¹): Co 7.41, C 51.38, H 7.22, N 8.81. Found: Co 7.65, C 51.10, H 6.70, N 9.10.

*Synthesis of (HNEt₃)₂[Co₂(H₂mpba)₃]-6DMF·5H₂O, **1b.*** CoCl₂·6H₂O (0.119 g, 0.5 mmol), H₄mpba·3H₂O (0.154 g, 0.5 mmol), and NEt₃ (99%, 0.28 mL, 2 mmol) were placed in a 23 mL Teflon-lined autoclave filled with DMF (9 mL) and heated at 100 °C for 12 h. After slow cooling to room temperature, red-brown crystals of **1b** were collected, washed by sonication in DMF, and dried in air. Yield: 0.043 g (11%, based on Co). IR (ATR, cm⁻¹): 3435 s; 3197 s; 3084 s; 1621 S; 1595 S; 1545 S; 1475 s; 1456 m; 1364 S; 1295 m; 1255 s; 1229 s; 1174 s; 1094 s; 1062 s; 1034 s; 988 s; 934 s; 892 s; 837 s; 799 S; 760 s; 689 s; 660 s; 598 s; 538 m; 517 s; 444 m; 405 s; 357 m; 307 S; 251 S; 214 m. Elemental analysis (%) calculated for C₆₀H₁₀₂Co₂N₁₄O₂₉ (*M*_r = 1601.39 g mol⁻¹): C 45.0, H 6.42, N 12.24. Found: C 44.65, H 6.06, N 12.46.

*Synthesis of TBA₂[Ni₂(H₂mpba)₃]-2DMF·2.5H₂O, **2.*** NiCl₂·6H₂O (0.119 g, 0.5 mmol), H₂Et₂mpba (0.154 g, 0.5 mmol), and TBAOH (1 M in MeOH, 1 mL, 1 mmol) were placed in a 23 mL Teflon-lined

autoclave filled with DMF (8 mL) and heated at 100 °C for 12 h. After slow cooling to room temperature, green crystals of **2** were collected, washed by sonication in DMF, and dried in air. Yield: 0.111 g (29%, based on Ni). IR (ATR, cm^{-1}): 3463 s; 3229 s; 3084 s; 2963 s; 2875 s; 1662 m; 1625 s; 1595 s; 1545 s; 1474 s; 1457 s; 1409 s; 1366 s; 1295 s; 1255 s; 1229 s; 1171 s; 1094 s; 1062 s; 1031 s; 988 s; 935 s; 894 s; 837 s; 802 m; 762 s; 739 s; 690 s; 660 s; 599 s; 540 s; 517 s; 499 s; 483 s; 462 s, 446 s; 406 s; 360 s, 318 m; 274 m. Elemental analysis (%) calculated for $\text{C}_{68}\text{H}_{109}\text{N}_{10}\text{Ni}_2\text{O}_{22.5}$ ($M_r = 1544 \text{ g mol}^{-1}$): Ni 7.60, C 52.89, H 7.11, N 9.07. Found: Ni 8.10, C 50.74, H 6.75, N 9.6.

Synthesis of $(\text{HNEt}_3)_2[\text{Co}_2(\text{H}_2\text{mpba})_3]$, **3.** $\text{CoCl}_2 \cdot 6\text{H}_2\text{O}$ (0.119 g, 0.5 mmol), $\text{H}_2\text{mpba} \cdot 3\text{H}_2\text{O}$ (0.153 g, 0.5 mmol), and NEt_3 (99%, 0.280 mL, 2 mmol) were placed in a 23 mL Teflon-lined autoclave filled with DMF (9 mL) and heated at 150 °C for 12 h. After slow cooling to room temperature, purple crystals of **3** were collected, washed by sonication in DMF, and dried in air. Yield: 0.135 g (50.3%, based on Co). IR (ATR, cm^{-1}): 3228 s; 1631 s; 1598 s; 1540 m; 1475 m; 1456 m; 1361 s; 1290 m; 1233 s; 1161 s; 1017 s; 979 s; 934 s; 885 s; 800 s; 707 s; 684 m; 630 s; 604 s; 545 m; 509 m; 439 m; 407 s; 358 s; 296 m; 273 s; 243 s. Elemental analysis (%) calculated for $\text{C}_{42}\text{H}_{50}\text{Co}_2\text{N}_8\text{O}_{18}$ ($M_r = 1072.75 \text{ g mol}^{-1}$): Co 10.98, C 47.02, H 4.69, N 10.44. Found: Co 10.66, C 47.56, H 4.64, N 10.66.

Crystallographic Studies. Data were collected on a Bruker Kappa-APEX II CCD diffractometer for **1b** and **3** (Mo $K\alpha$, $\lambda = 0.71073 \text{ \AA}$). Crystals were mounted on a Hamilton cryoloop using Paratone-N oil and placed in the cold flow produced with an Oxford Cryocooling device. Partial hemispheres of data, predefined with the APEX II software,^{28a} were collected using ϕ and ω scans (110 s/frame for **1b**, 100 s/frame for **3**). Integrated intensities were obtained with SAINT+^{28a} and were corrected for absorption with SADABS,^{28b,c} structure solution and refinement was performed with the SHELXTL-package.^{28a} The structures were solved by direct methods and completed by iterative cycles of ΔF syntheses and full-matrix least-squares refinement against F^2 . Compounds **1a**, **1b**, and **2** are poorly diffracting, and despite numerous efforts, the best data set obtained, for **1b**, still gives some large reliability factors, and restraints have been used to model counterions and solvent molecules. Crystallographic data and refinement parameters for **1b** and **3** are given in Table 1.

X-ray powder diffraction patterns for **1a**, **1b**, and **2** are presented in the Figure S1 of the Supporting Information. Diagrams were collected on a Philips X'pert Pro diffractometer using Cu $K\alpha_1$ monochromatized radiation ($\lambda = 1.54060 \text{ \AA}$) and equipped with an X'celerator linear detector.

RESULTS

Compounds **1a**, **1b**, and **2** are isostructural and crystallize in the $R\bar{3}c$ centrosymmetric space group with an asymmetric unit that consists of one-sixth of the bimetallic complex. Each complex is made of two divalent ions in octahedral geometry bridged by three partially deprotonated $(\text{H}_2\text{mpba})^{2-}$ ligands. The metal ions bind two oxygen atoms from the oxamate groups leaving one carbonyl and one amido function uncoordinated. Such a binding mode arises from the nondeprotonation of the amido groups independently of the strength of the base used in the reaction and results in the formation of a triple-stranded chiral helicate complex where the oxamate groups lie in the plane of the benzyl rings (Figure 1b).

The formation of multiple hydrogen bonds between the amide (proton donor) and carbonyl (proton acceptor) functions of oxamic acids from adjacent complexes leads to a 3D framework composed of 2D hexagonal layers pillared by the helicoidal complexes (Figure 1c and 2). The found N(\cdots H) \cdots O distance of 2.81(1) \AA is relatively short in comparison to the intermolecular H-bond distances reported for the $\text{H}_2\text{Et}_2\text{mpba}$ ligand.^{29,30} The 2D (6,3) hexagonal networks are composed of cobalt octahedra linked via their edges by double H-bonds through the oxamate groups, and it is now well

Table 1. Crystallographic Data for Compounds **1b** and **3**

	1b	3
formula ^a	$\text{C}_{51}\text{H}_{91}\text{Co}_2\text{N}_{11}\text{O}_{31}$	$\text{C}_{42}\text{H}_{50}\text{Co}_2\text{N}_8\text{O}_{18}$
FW [g mol^{-1}]	1472.21	1072.76
cryst syst	trigonal	monoclinic
space group	$R\bar{3}c$	$P2_1$
<i>a</i> [\AA]	17.527(7)	10.3375(6)
<i>b</i> [\AA]	17.527(7)	15.2574(15)
<i>c</i> [\AA]	46.452(7)	15.0870(15)
α [deg]	90	90
β [deg]	90	91.745(7)
γ [deg]	120	90
<i>V</i> [\AA^3]	12359(3)	2378,5(4)
<i>Z</i>	6	2
<i>T</i> [K]	200(2)	200(2)
λ [\AA]	0.71073	0.71073
ρ_{calc} [g cm^{-3}]	1.187	1.498
$\mu(\text{Mo } K\alpha)$ [mm^{-1}]	0.480	0.780
<i>F</i> (000)	4656	1112
cryst size [mm^3]	$0.32 \times 0.19 \times 0.17$	$0.31 \times 0.15 \times 0.15$
θ limits [deg]	2.21–24.99	3.01–30.01
meas reflns	19834	28005
unique reflns	2416	12872
R_{int}	0.0960	0.0345
reflections $I > 2\sigma(I)$	1595	9744
params	124	633
restraints	9	1
R_1^b [$I > 2\sigma(I)$]	0.0849	0.0422
wR_2^c	0.2981	0.0955
GOF	1.135	1.000
largest residuals [e \AA^{-3}]	−0.543; 1.823	−0.319; 0.429

^aIncluding solvate molecules. ^b $R_1 = \sum ||F_o| - |F_c|| / \sum |F_o|$. ^c $wR_2 = [\sum (\omega(F_o^2 - F_c^2)^2) / \sum (\omega(F_o^2))]^{1/2}$.

established that a 2D net made of octahedra sharing edges is only obtained for a perfect alternation of Λ and Δ isomers.^{31–33} (On the other hand, a 3D (10,3) chiral framework is obtained for enantiopure octahedra sharing edges; see, for instance, ref 33.) Therefore both enantiomers of the helicate are found in the structure and are alternatively linked to one another through the double H-bonds to yield the heterochiral honeycomb-like framework $A_4[\Delta\text{-M}\Delta\text{-M}(\text{H}_2\text{mpba})_3][\Lambda\text{-M}\Lambda\text{-M}(\text{H}_2\text{mpba})_3]$ ($A = \text{TBA}^+$, HNEt_3^+ ; $M = \text{Ni}$, Co) (Figure 2). It is worth noticing that the H-bonds seem to solely drive the three-dimensional arrangement of the complexes since no obvious structural differences could be observed between the TBA^+ and the HNEt_3^+ salts. The formation of this relatively strong supramolecular network could potentially tend to stabilize the helicate complex and limit the deprotonation of the ligands.

This binding mode of the $(\text{H}_x\text{mpba})^{(4-x)-}$ ligand is encountered for the first time. Indeed, under bench conditions and in aqueous media, the fully deprotonated form of the ligand, $(\text{mpba})^{4-}$, also binds octahedral ions in a 3:2 fashion but affords a heterochiral triple-stranded mesocate bimetallic complex $[\text{Co}_2(\text{mpba})_3]^{8-}$ where the oxamate groups are perpendicular to the benzyl rings (Figure 3a).²⁰ This difference in the geometrical arrangement in **1b** and in $[\text{Co}_2(\text{mpba})_3]^{8-}$ changes the relative orientation of the coordination polyhedra between the two halves of the dinuclear complexes. In **1b**, the two polyhedra have a staggered conformation when viewed along the Co–Co axis, whereas in $[\text{Co}_2(\text{mpba})_3]^{8-}$ the two

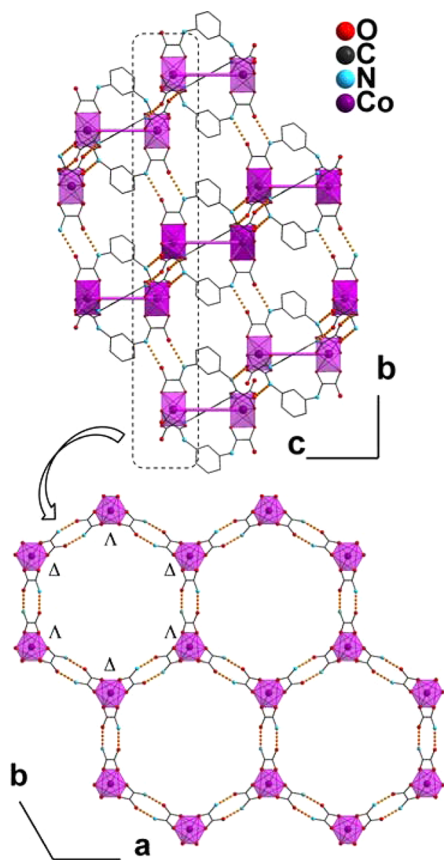


Figure 2. Crystal packing of **1b** showing the H-bond structuring (orange dotted lines) into a heterochiral hexagonal 3D network; H atoms are omitted for clarity; dinuclear complexes are schemed with an intramolecular Co–Co bond pictured in purple in the *bc* plane; benzyl rings are omitted for clarity in the representation of the *ab* plane.

polyhedra have an eclipsed conformation (Figure 3b,c). Consequently these conformations lead to different networks. In **1b**, the double H-bonds between adjacent complexes lead to a stacking of staggered hexagonal networks (Figure 4a) with the same topology as diamond or sphalerite structures, that is, “dia” net in RCSR database,^{3,4} whereas in $\text{Li}_5[\text{Li}_3\text{Co}_2(\text{mpba})_3(\text{H}_2\text{O})_6] \cdot 31\text{H}_2\text{O}$, the coordination of the two cis carbonyl-oxygen atoms of the oxamato groups to Li^+

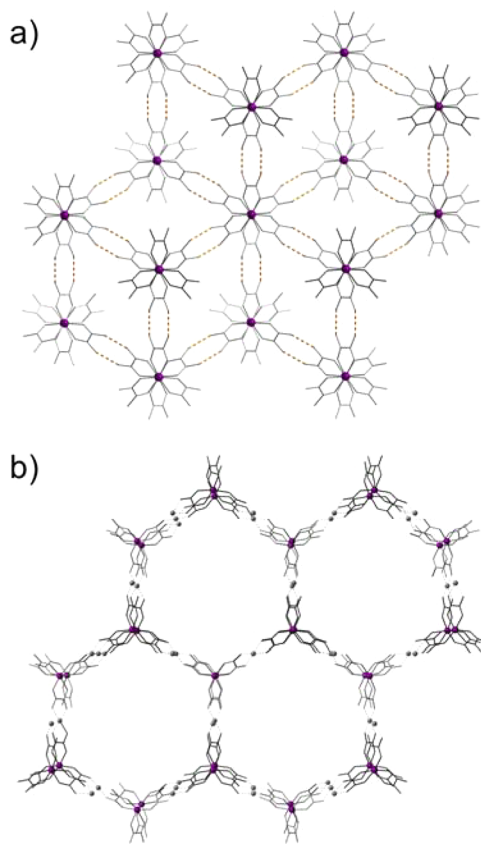


Figure 4. Stacking of hexagonal networks in (a) **1b** and (b) $[\text{Li}_3\text{Co}_2(\text{mpba})_3(\text{H}_2\text{O})_6]^{5-}$; benzyl rings are omitted for clarity.

ions leads to a 3D honeycomb framework with hexagonal channels and is topologically like the lonsdaleite or wurtzite structures, that is, “lon” in RCSR database. By contrast, the staggered conformation of the helicate does not lead to large pores in **1b**.

Compound **3** crystallizes in the $P2_1$ chiral space group, and a whole complex is found in the asymmetric unit. The bimetallic complex is identical to the previously described compounds; however, there are drastic differences in the 3D layout since the H-bond-driven arrangement of the bimetallic species leads to a homochiral framework (Figure 5). The H-bond network is far more complex than in the previous cases with each ligand of the

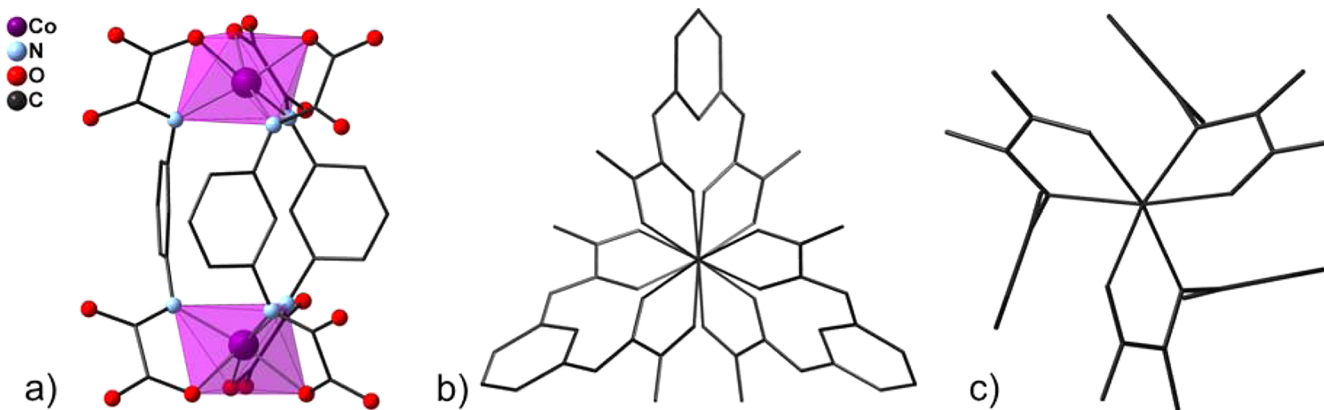


Figure 3. (a) Structure of the anionic complex $[\text{Co}_2(\text{mpba})_3]^{8-20}$; (b) stick model of **1b** along the Co–Co axis; (c) Stick model of $[\text{Co}_2(\text{mpba})_3]^{8-}$ along the Co–Co axis.

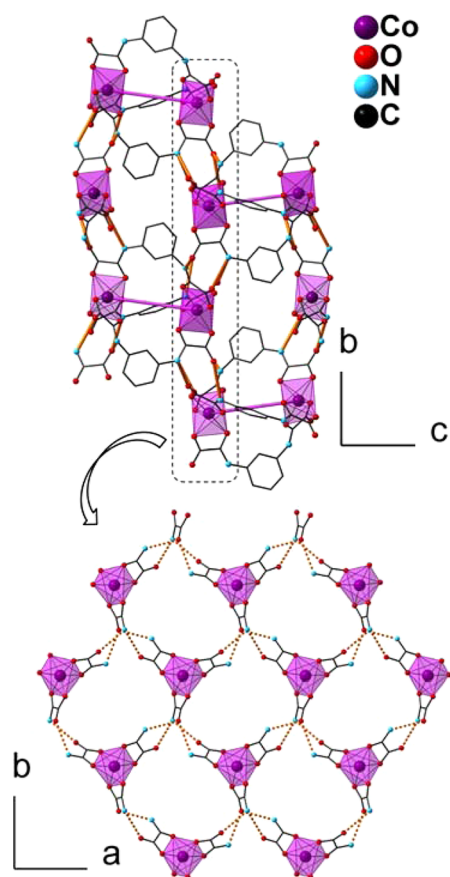


Figure 5. Crystal packing of **3** showing the H-bond structuring (orange dotted lines) into a homochiral 3D network; H atoms are omitted for clarity; dinuclear complexes are schemed with an intramolecular Co–Co bond pictured in purple in the *bc* plane; benzyl rings are omitted for clarity in the representation of the *ab* plane.

same molecular unit displaying a different H-bonding mode to two or three adjacent molecules (Figure 6). Triethylammonium cations also form hydrogen bonds with the carbonyl groups of the ligand and are located in the cavities of the distorted hexagonal architecture defined by the metallic complexes (Figure S2 in the Supporting Information). The intermolecular N(–H)⋯O distances found in the structure range from

2.8708(2) to 3.0886(3) Å with a mean value of 2.97 Å. One can suppose that performing the reaction at 150 instead of 100 °C leads to a higher autogenous pressure during the solvothermal treatment, which in turn constrains the system to stabilize into a denser phase and hence this more complex H-bond networking. The consequence of this densification is the lack of one of the two enantiomers of the bis-cobalt(II) helicate in the hexagonal lattice. Although distorted, the hexagonal lattice is still visible in Figure 5 with vertices alternatively defined by cobalt octahedra and the entanglement of hydrogen bonds leading then to an enantiopure network.

No signals were found in circular dichroism measurements performed on the bulk material indicating that both enantiomers (HNEt₃)₂[Δ-CoΔ-Co(H₂mpba)₃] and (HNEt₃)₂[Λ-CoΛ-Co(H₂mpba)₃] crystallize out from the solvothermal reaction. Attempts to measure circular dichroism data on a single crystal diluted in KBr proved unsuccessful whereas measurements in solution were made impossible because compound **3** is insoluble in most common solvents, including DMSO or DMF.

Magnetic Properties. Magnetic measurements in DC mode were performed on all compounds (Figure 7). At room temperature, the $\chi_M T$ values, approximately 6.5 cm³·K·mol⁻¹ for **1a**, **1b**, and **3**, are close to the expected one for two isolated Co(II) ions. Upon cooling, the $\chi_M T$ products steadily decrease and reach 3.7 cm³·K·mol⁻¹ at 2 K. In the 300–2 K temperature range, the experimental curves can be modeled using the theoretical behavior of two isolated distorted octahedral cobalt(II) ions.³⁵ The best fit of the data obtained by full-matrix diagonalization of the appropriate spin Hamiltonian gave $\lambda = -128$ cm⁻¹, $D = -391$ cm⁻¹, and $\alpha = 0.99$ for **1a**; $\lambda = -179$ cm⁻¹, $D = -565$ cm⁻¹, and $\alpha = 0.76$ for **1b**; and $\lambda = -168$ cm⁻¹, $D = -494$ cm⁻¹, and $\alpha = 0.79$ for **3**, where λ , D , and α are the spin orbit coupling constant, the distortion parameter, and the orbital reduction factor, respectively. The theoretical curves reproduce quite well the experimental data over the whole range of temperature showing that there is no interaction between the cobalt ions within the helicates. For the bis-nickel helicate **2**, the $\chi_M T$ value remains constant in the 300–100 K temperature range and is equal to 2.2 cm³·K·mol⁻¹, which is close to the expected one for two magnetically isolated Ni(II) ions. Below 100 K, the value of $\chi_M T$ slowly decreases to reach a value of 1.9 cm³·K·mol⁻¹ at 2 K. This behavior could be interpreted either by a very weak interaction between the two

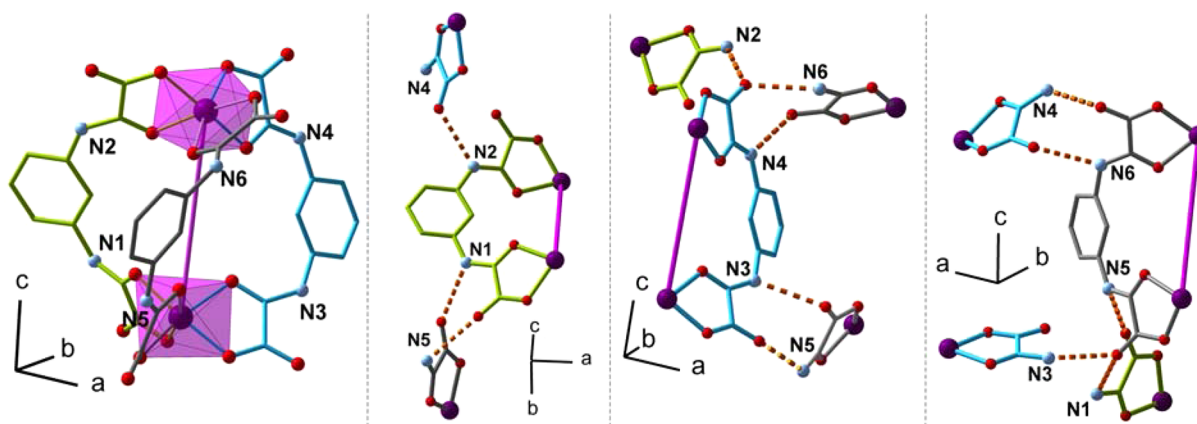


Figure 6. Schematic view of the N(–H)⋯O bonds (orange dotted lines) between adjacent molecules in **3**; H atoms are omitted for clarity; the dinuclear complex is schemed with an intramolecular Co–Co bond pictured in purple.

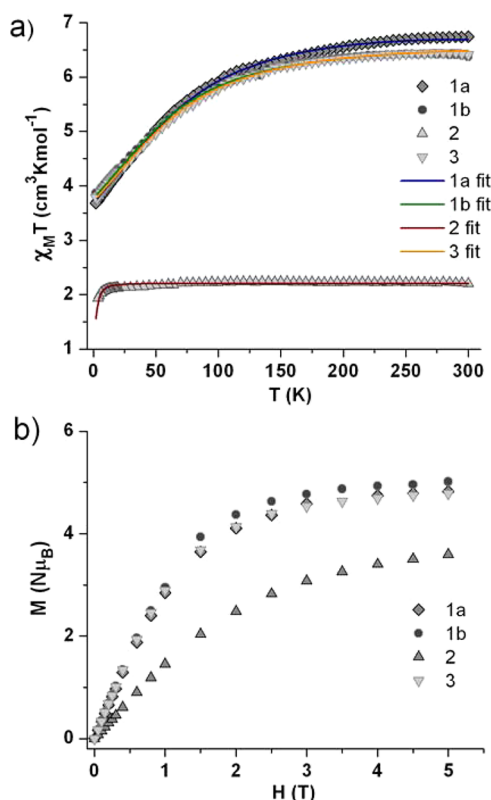


Figure 7. (a) Plots of $\chi_M T$ vs T measured from 300 to 2 K at 1 kOe for 1a (◆), 1b (●), 2 (▲), and 3 (▼) and respective fits in solid lines: 1a, blue; 1b, green; 2, red; 3, orange. (b) Plots of M vs H measured from 0 to 7 T at 2 K for 1a (◆), 1b (●), 2 (▲), and 3 (▼).

Ni(II) ions within the helicate or by the effect of the zero field splitting of the individual Ni(II) ions. The best data fits gave $g = 2.1$, $J = -0.6 \text{ cm}^{-1}$ for the first model and $g_{\text{Ni}} = 2.1$ and $D_{\text{Ni}} = -6.5 \text{ cm}^{-1}$ for the second one. The agreement factor $R = [(\chi_M T)_{\text{exp}} - (\chi_M T)_{\text{calcd}}]^2 / [(\chi_M T)_{\text{exp}}]^2$ is slightly better for the first model with values equal to $R = 10^{-4}$ and 2×10^{-4} , respectively. However, the lack of interaction in the cobalt-based helicates leads us to favor the second model.

The lack of interaction in these helicates contrasts with the results obtained for the cobalt and nickel mesocates, in which the (mpba)⁴⁻ ligand is deprotonated, where a weak but noticeable ferromagnetic interaction is observed with $J = 1 \text{ cm}^{-1}$ and $J = 3.6 \text{ cm}^{-1}$, respectively.^{20,36} This difference in the magnetic behavior is explained by the relative orientation of oxamate groups with the benzene rings. In the helicate family, the oxamate groups are almost in the same plane as the benzene cycles. As a consequence, the interaction between the magnetic orbitals of the cobalt or nickel ions and the π orbitals of the benzene rings is very weak, and there is no efficient pathway with the σ bonds of the benzene rings. In contrast, in the mesocates the oxamate groups are perpendicular to the benzene ring; this conformation allows a σ overlap between the e_g magnetic orbitals and the lone pair of the deprotonated amide nitrogen atom, which are in strong interaction with the extended π conjugated bond system of the phenylene spacers.³⁷ This situation leads to a quite large spin polarization effect through the π orbitals of the benzene rings, and despite a metal–metal distance that goes up to 6.85 \AA , which is actually longer than in the case of the helicates, there is a magnetic interaction in the mesocate family. The simple protonation or

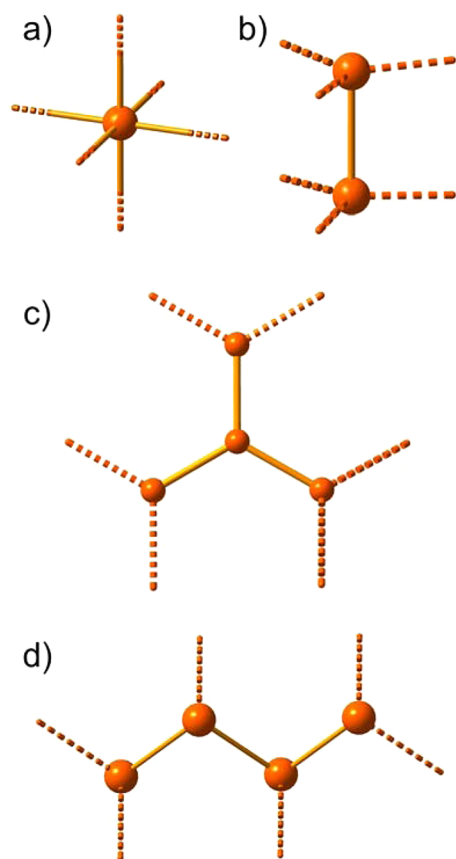
deprotonation of the mpba ligands completely changes the magnetic properties of the dinuclear compounds from ferromagnetic coupling to an uncoupled system, and this is a perfect illustration that the important parameter in the exchange interaction is not primarily the metal–metal distance but the existence of molecular orbitals able to transmit the interaction.

DISCUSSION

Unexpectedly, solvothermal synthesis using polyoxalamide ligands has led to new coordination compounds with ligands bearing double H-bonds sites. These complexes are built from metal ions and partially protonated ligands comprising oxamide anions. Oxamide anions are known to be flexible building blocks for hydrogen-bonded architectures.³⁸ Indeed, the compounds presented in this paper are interesting examples of networks built simultaneously from coordination complexes and complementary hydrogen bonding sites.^{39–41} In inorganic crystal engineering, this strategy is, in theory, very effective. The geometrical preferences of the coordination sphere of the metal ions (square planar, octahedral, etc.) induce a precise orientation of hydrogen-bonding groups that can also propagate geometrical information, which would lead, in principle, to predictable results. In practice, the situation is less clear. For instance, with 2,2-bisimidazolato tris-chelate complex building blocks, the directions of the H-bonds are coplanar and separated by an angle of 120° , so the obvious construction is a honeycomb network, and some results confirm this expectation.⁴² However, there are several examples of more complicated structures that include interpenetrating nets⁴² and achiral,⁴³ racemate,⁴⁴ and chiral 3D structures.⁴⁵ Even, 0D, 1D zigzag, and 1D helical structures were obtained.^{43,46} Switching from one structure to another depends on other subtle intermolecular interactions, such as the role of the counterions or the control of the chirality of the metal-ion coordination sphere. Therefore, whatever the type of connection used to form a network either by hydrogen bonds or by coordination bonds, if tris-chelate complex building blocks appear as a reliable way to obtain self-organized 2D or 3D nets, the final dimensionality remains difficult to predict. This is especially true for 3D nets because they seem difficult to achieve although it is not completely unexpected since a basic unit bearing six connecting points is necessary to build a 3D net by translation.^{47,48} Consequently, a tris-chelate building block with only three connecting points does not meet this requirement. Since the basic unit must be connected to six others, it is then compulsory to have at least four tris-chelates in the basic unit in order to build a three-connected 3D net, that is, a tetranuclear complex as building block (Scheme 1). In the case of monomeric metal complexes, only an octahedral complex with six bis-monodentate ligands like hexacyanometallates is able to build a 3D network.^{49,50} For dinuclear building blocks, it is necessary to have a connectivity of four at each node to obtain 3D networks, and the helicates described in this paper meet this requirement.

Actually, these new helicate complexes bearing six double H-bonds sites illustrate nicely the “recipe” A.F. Wells proposed in the 1950s to build a 3D four-connected net,^{51,52} “The simplest planar 3-connected net is the hexagonal net with 2 points in the repeat unit. By connecting alternate points to points in layers above and below there arises the simplest three-dimensional 4-connected net.” This description corresponds to the exact structure of compound 1b. Furthermore, owing to the structure

Scheme 1. Simplest Building Blocks Providing the Six Necessary Connecting Points To Build 3D Nets: (a) Mononuclear, (b) Dinuclear, and (c, d) Tetranuclear



of the helicate, the resulting net in **1b** was perfectly predictable. However, it should be noted that the structure of **3** with the entanglement of hydrogen bonds that results from a temperature effect was not anticipated even though the same initial synthon is present. To summarize, the dinuclear triple-stranded helicates or mesocates are perfect building blocks to obtain 3D networks because they offer the six required connecting points. It is worth noting that the polynuclear complexes $\{Zn_4O(RCO_2)_6\}$ and $\{Cr_3O(RCO_2)_6\}$ which are used as SBUs (secondary building units) in 3D MOF **5**⁵³ and MIL 101⁵⁴ also possess six connecting points.

CONCLUSION

Solvothermal synthesis has successfully led to novel chiral helicate oxamate-based dinuclear complexes where supra-molecular H-bond networking in the solid influenced by the synthesis temperature leads to 3D diamond-like or 3D chiral structures. From these results obtained fortuitously, it is possible to conclude that, as in the synthesis of MOF, the use of polynuclear metal complexes as building blocks is a good strategy to build 3D networks in a predictable and controlled way. To the best of our knowledge, the strategic use of discrete polymetallic coordination compounds bearing hydrogen bond sites specifically designed to construct networks rationally has not been explored so far in crystal engineering, and the present results open a synthetic route that is worth following. There had been no example of oxamate-based coordination compounds obtained solvothermally, and this preliminary

study is thus promising. Indeed the use of solvothermal conditions combined with the rich family of ligands that oxamate derivatives constitute clearly opens a new synthetic route toward multidimensional molecular magnetic materials.

ASSOCIATED CONTENT

Supporting Information

X-ray crystallographic files for **1b** and **3** in CIF format and figures showing experimental X-ray powder diffraction patterns for **1a**, **1b**, and **2** and calculated patterns for **1a** and **1b**, and intermolecular hydrogen bonds between the bimetallic complex and its $HNEt_3^+$ counterions in **3**. This information is available free of charge via the Internet at <http://pubs.acs.org>.

AUTHOR INFORMATION

Corresponding Author

*Phone: +33 1 44 27 55 62. Fax: +33 1 44 27 38 41. E-mail: yves.journaux@upmc.fr.

Notes

The authors declare no competing financial interest.

ACKNOWLEDGMENTS

This work was supported by the Ministère de la Recherche et de l'Enseignement Supérieur (MRES) and the Centre National de la Recherche Scientifique (CNRS).

REFERENCES

- (1) Aakeroy, C. B.; Champness, N. R.; Janiak, C. *CrystEngComm* **2010**, *12*, 22–43.
- (2) Robson, R. J. *Chem. Soc., Dalton Trans.* **2000**, 3735–3744.
- (3) Fujita, M. *Chem. Soc. Rev.* **1998**, *27*, 417–425.
- (4) Swiegers, G. F.; Malefetse, T. J. *Chem. Rev.* **2000**, *100*, 3539–3539.
- (5) Chakrabarty, R.; Mukherjee, P. S.; Stang, P. J. *Chem. Rev.* **2011**, *111*, 6810–6918.
- (6) Long, J. R.; Yaghi, O. M. *Chem. Soc. Rev.* **2009**, *38*, 1213–1214.
- (7) Murray, L. J.; Dinca, M.; Long, J. R. *Chem. Soc. Rev.* **2009**, *38*, 1294–1314.
- (8) Sumida, K.; Rogow, D. L.; Mason, J. A.; McDonald, T. M.; Bloch, E. D.; Herm, Z. R.; Bae, T.-H.; Long, J. R. *Chem. Rev.* **2012**, *112*, 724–781.
- (9) Allendorf, M. D.; Bauer, C. A.; Bhakta, R. K.; Houk, R. J. T. *Chem. Soc. Rev.* **2009**, *38*, 1330–1352.
- (10) Cui, Y.; Yue, Y.; Qian, G.; Chen, B. *Chem. Rev.* **2012**, *112*, 1126–1162.
- (11) Zhang, W.; Xiong, R.-G. *Chem. Rev.* **2012**, *112*, 1163–1195.
- (12) Kurmoo, M. *Chem. Soc. Rev.* **2009**, *38*, 1353–1379.
- (13) Coffman, R. E.; Buettner, G. R. *J. Phys. Chem.* **1979**, *83*, 2387–2392.
- (14) Pardo, E.; Carrasco, R.; Ruiz-Garcia, R.; Julve, M.; Lloret, F.; Munoz, M. C.; Journaux, Y.; Ruiz, E.; Cano, J. *J. Am. Chem. Soc.* **2008**, *130*, 576–585.
- (15) Fernandez, I.; Ruiz, R.; Faus, J.; Julve, M.; Lloret, F.; Cano, J.; Ottenwälder, X.; Journaux, Y.; Munoz, M. C. *Angew. Chem., Int. Ed.* **2001**, *40*, 3039–3042.
- (16) Dul, M. C.; Pardo, E.; Lescouezec, R.; Chamoreau, L. M.; Villain, F.; Journaux, Y.; Ruiz-Garcia, R.; Cano, J.; Julve, M.; Lloret, F.; Pasan, J.; Ruiz-Perez, C. *J. Am. Chem. Soc.* **2009**, *131*, 14614–14615.
- (17) Pardo, E.; Ferrando-Soria, J.; Dul, M.-C.; Lescouezec, R.; Journaux, Y.; Ruiz-García, R.; Cano, J.; Julve, M.; Lloret, F.; Cañadillas-Delgado, L.; Pasán, J.; Ruiz-Pérez, C. *Chem.—Eur. J.* **2010**, *16*, 12838–12851.
- (18) Dul, M. C.; Ottenwälder, X.; Pardo, E.; Lescouezec, R.; Journaux, Y.; Chamoreau, L. M.; Ruiz-Garcia, R.; Cano, J.; Julve, M.; Lloret, F. *Inorg. Chem.* **2009**, *48*, 5244–5249.

- (19) Pereira, C. L. M.; Pedroso, E. F.; Stumpf, H. O.; Novak, M. A.; Ricard, L.; Ruiz Garcia, R.; Riviere, E.; Journaux, Y. *Angew. Chem., Int. Ed.* **2004**, *43*, 955–958.
- (20) Pardo, E.; Cangussu, D.; Dul, M.-C.; Lescouezec, R.; Herson, P.; Journaux, Y.; Pedroso, E. F.; Pereira, C. L. M.; Muñoz, M. C.; Ruiz-Garcia, R.; Cano, J.; Amorós, P.; Julve, M.; Lloret, F. *Angew. Chem., Int. Ed.* **2008**, *47*, 4211–4216.
- (21) Ferrando-Soria, J.; Ruiz-Garcia, R.; Cano, J.; Stiriba, S. E.; Vallejo, J.; Castro, L.; Julve, M.; Lloret, F.; Amoros, P.; Pasan, J.; Ruiz-Perez, C.; Journaux, Y.; Pardo, E. *Chem.—Eur. J.* **2012**, *18*, 1608–1617.
- (22) Laudise, R. A. *Chem. Eng. News* **1987**, *65*, 30–43.
- (23) Rabenau, A. *Angew. Chem., Int. Ed.* **1985**, *24*, 1026–1040.
- (24) Férey, G. *Chem. Mater.* **2001**, *13*, 3084–3098.
- (25) Rosi, N. L.; Eddaoudi, M.; Kim, J.; O’Keeffe, M.; Yaghi, O. M. *CrystEngComm* **2002**, 401–404.
- (26) Laye, R. H.; McInnes, E. J. L. *Eur. J. Inorg. Chem.* **2004**, *2004*, 2811–2818.
- (27) Cervera, B.; Sanz, J. L.; Ibanez, M. J.; Vila, G.; Lloret, F.; Julve, M.; Ruiz, R.; Ottenwaelder, X.; Aukauloo, A.; Poussereau, S.; Journaux, Y.; Munoz, M. C. *J. Chem. Soc., Dalton Trans.* **1998**, 781–790.
- (28) (a) BrukerAXS Inc, Madison, Wisconsin, USA, 1998. (b) Sheldrick, G. M. *Acta Crystallogr.* **2008**, *A64*, 112. (c) Blessing, R. H. *Acta Crystallogr.* **1995**, *A51*, 33.
- (29) Blay, G.; Fernández, I.; Pedro, José, R.; Ruiz-García, R.; Muñoz, M. C.; Cano, J.; Carrasco, R. *Eur. J. Org. Chem.* **2003**, 1627–1630.
- (30) Padilla-Martinez, I. I.; Chaparro-Huerta, M.; Martinez-Martinez, F. J.; Hopfl, H.; Garcia-Baez, E. V. *Acta Crystallogr.* **2003**, *E59*, O825–O827.
- (31) Tamaki, H.; Zhong, Z. J.; Matsumoto, N.; Kida, S.; Koikawa, M.; Achiwa, N.; Okawa, H. *J. Am. Chem. Soc.* **1992**, *114*, 6974–6979.
- (32) Decurtins, S. *Inorg. Chim. Acta* **1994**, *216*, 65.
- (33) Gruselle, M.; Train, C.; Boubekeur, K.; Gredin, P.; Ovanesyan, N. *Coord. Chem. Rev.* **2006**, *250*, 2491–2500.
- (34) O’Keeffe, M.; Peskov, M. A.; Ramsden, S. J.; Yaghi, O. M. *Acc. Chem. Res.* **2008**, *41*, 1782–1789.
- (35) Lloret, F.; Julve, M.; Cano, J.; Ruiz-García, R.; Pardo, E. *Inorg. Chim. Acta* **2008**, *361*, 3432–3445.
- (36) Pardo, E.; Morales Osorio, I.; Julve, M.; Lloret, F.; Cano, J.; Ruiz Garcia, R.; Pasan, J.; Ruiz Perez, C.; Ottenwaelder, X.; Journaux, Y. *Inorg. Chem.* **2004**, *43*, 7594–7596.
- (37) Pardo, E.; Ruiz-Garcia, R.; Cano, J.; Ottenwaelder, X.; Lescouezec, R.; Journaux, Y.; Lloret, F.; Julve, M. *Dalton Trans.* **2008**, 2780–2805.
- (38) Aakeroy, C. B.; Hughes, D. P.; Nieuwenhuyzen, M. *J. Am. Chem. Soc.* **1996**, *118*, 10134–10140.
- (39) Burrows, A. D.; Chan, C.-W.; Chowdhry, M. M.; McGrady, J. E.; Mingos, D. M. P. *Chem. Soc. Rev.* **1995**, 24.
- (40) Tadokoro, M.; Nakasujii, K. *Coord. Chem. Rev.* **2000**, *198*, 205–218.
- (41) Brammer, L. *Chem. Soc. Rev.* **2004**, *33*, 476–489.
- (42) Tadokoro, M.; Isobe, K.; Uekusa, H.; Ohashi, Y.; Toyoda, J.; Tashiro, K.; Nakasujii, K. *Angew. Chem., Int. Ed.* **1999**, *38*, 95–98.
- (43) Öhrström, L.; Larsson, K.; Borg, S.; Norberg, S. T. *Chem.—Eur. J.* **2001**, *7*, 4805–4810.
- (44) Tadokoro, M.; Shiomi, T.; Isobe, K.; Nakasujii, K. *Inorg. Chem.* **2001**, *40*, 5476–5478.
- (45) Larsson, K.; Öhrstrom, L. *CrystEngComm* **2003**, *5*, 222–225.
- (46) Tadokoro, M.; Kanno, H.; Kitajima, T.; Shimada-Umemoto, H.; Nakanishi, N.; Isobe, K.; Nakasujii, K. *Proc. Natl. Acad. Sci. U.S.A.* **2002**, *99*, 4950–4955.
- (47) Wells, A. F. *Acta Crystallogr.* **1954**, *7*, 535–544.
- (48) Öhrstrom, L.; Larsson, K. *Dalton Trans.* **2004**, 347–353.
- (49) Buser, H. J.; Schwarzenbach, D.; Petter, W.; Ludi, A. *Inorg. Chem.* **1977**, *16*, 2704–2710.
- (50) Witzel, M.; Babel, D. *Acta Crystallogr.* **1984**, *A40*, C216–C216.
- (51) Wells, A. F. *Acta Crystallogr.* **1954**, *7*, 545–554.
- (52) Wells, A. F. *Structural Inorganic Chemistry*; Clarendon Press: Oxford, 1984.
- (53) Li, H.; Eddaoudi, M.; O’Keeffe, M.; Yaghi, O. M. *Nature* **1999**, *402*, 276.
- (54) Férey, G.; Mellot-Draznieks, C.; Serre, C.; Millange, F.; Dutour, J.; Surlblé, S.; Margiolaki, I. *Science* **2005**, *309*, 2040–2042.